An Atmospheric Correction Algorithm for Remote Sensing of Bright Coastal Waters Using MODIS Land and Ocean Channels in the Solar Spectral Region

Bo-Cai Gao, Marcos J. Montes, Rong-Rong Li, Heidi Melita Dierssen, and Curtiss O. Davis

***Abstract*—The present operational atmospheric correction algorithm for multichannel remote sensing of ocean color using imaging data acquired with the Moderate Resolution Imaging Spectroradiometer (MODIS) works well over clear ocean but can give incorrect results over brighter coastal waters. This is because: 1) the turbid waters are not dark for the two atmospheric correction channels centered near 0.75 and 0.86 μm; and 2) the ocean color channels (0.488, 0.531, and 0.551 μm) often saturate over bright coastal waters. Here, we describe an atmospheric correction algorithm for multichannel remote sensing of coastal waters. This algorithm is a modification of our previously developed atmospheric correction algorithm for hyperspectral data that uses lookup tables generated with a vector radiative transfer code and multilayered atmospheric models. Aerosol models and optical depths are determined by a spectrum-matching technique utilizing channels located at wavelengths longer than 0.86 μm, where the ocean surface is dark. The aerosol information in the visible spectral region is estimated based on the derived aerosol models and optical depths. Water-leaving radiances in the visible spectral region are obtained by subtracting out the atmospheric path radiances from the satellite-measured total radiances. Applications of the algorithm to two MODIS data sets are presented and compared to field measurements. The water-leaving reflectances retrieved with this algorithm over brighter shallow coastal waters compare closely with those from field measurements. In addition, the retrieved water-leaving reflectances over deeper ocean waters compare well with those derived with the MODIS operational algorithm.**

***Index Terms*—Coastal water, Moderate Resolution Imaging Spectroradiometer (MODIS), ocean color, remote sensing.**

I. INTRODUCTION

MULTICHANNEL remote sensing of ocean color from space has a rich history—from the past Coastal Zone Color Scanner (CZCS) [1], to Sea-viewing Wide Field-of-View Sensor (SeaWiFS) [2], and to the present Moderate Resolution Imaging Spectroradiometer (MODIS) instruments [3], [4] on the NASA Terra and Aqua spacecrafts. Among ocean color sensors, CZCS, Ocean Color and Temperature Scanner [5], and SeaWiFS were originally designed exclusively for ocean color applications. MODIS is a multipurpose NASA facility instrument designed for the global remote sensing of land, ocean, and atmosphere.

The atmospheric correction algorithms for processing remotely sensed data from these sensors were primarily designed for retrieving water-leaving radiances in the visible spectral region over deep ocean areas where phytoplankton is the dominant water constituent ("Case 1" waters) [6], [7]. The information about atmospheric aerosols is derived from channels centered near 0.66, 0.75, and 0.86 μm, where the water-leaving radiances are close to zero. The aerosol information is derived by extrapolation from the near infrared (IR) to the visible part of the spectrum. For turbid coastal environments and optically shallow waters ("Case 2" waters) [8], water-leaving radiances for channels near 0.66 and 0.75 μm may be significantly greater than zero because of backscattering by suspended materials in the water and bottom reflectance. Hence, these channels cannot be used for deriving information on atmospheric aerosols. Applications of the Case 1 algorithm to satellite imagery acquired over turbid coastal waters often result in negative water-leaving radiances over extended areas. At present, operational products over optically shallow waters are not produced. Therefore, improved atmospheric correction algorithms must be developed for the remote sensing of Case 2 waters.

Previously, we developed an atmospheric correction algorithm for hyperspectral remote sensing of ocean color [9]. In this paper, we describe modifications to this algorithm for multichannel remote sensing of coastal waters using MODIS channels in the 0.4–2.5 μm solar spectral region. We apply the algorithm to MODIS imagery obtained over optically shallow waters of the Bahamas Banks and Florida Bay. We compare the retrieved water-leaving reflectances with those from field measurements and with those derived with the MODIS operational atmospheric correction algorithm.

II. BACKGROUND

MODIS has 36 channels located in a wide spectral range from about 0.4–14.3 μm for remote sensing of land, ocean, and

Manuscript received September 8, 2006; revised January 10, 2007. This work was supported in part by the NASA SIMBIOS Project Office, Goddard Space Flight Center, U.S. Office of Naval Research, NASA Ocean Biology and Biogeochemistry (H. M. Dierssen), National Science Foundation Chemical Oceanography (R. C. Zimmerman).

B.-C. Gao, M. J. Montes, and R.-R. Li are with the Remote Sensing Division, Naval Research Laboratory, Washington, DC 20375 USA (e-mail: gao@nrl.navy.mil).

H. M. Dierssen is with the Department of Marine Sciences, University of Connecticut, Groton, CT 06340 USA.

C. O. Davis is with the College of Oceanic and Atmospheric Sciences, Oregon State University, Corvallis, OR 97331-5503 USA.

Digital Object Identifier 10.1109/TGRS.2007.895949

TABLE I
MAIN CHARACTERISTICS OF MODIS LAND AND OCEAN COLOR CHANNELS IN THE VISIBLE AND NEAR-IR SPECTRAL REGIONS

Primary Use	Channel	Bandwidth (nm)	Maximum Reflectance	Signal to Noise Ratio
Land/Cloud	1	620 – 670	1.49	128
	2	841 – 876	1.00	201
	3	459 – 479	1.04	243
	4	545 – 565	0.93	228
	5	1230 – 1250	0.51	74
	6	1628 – 1652	1.02	275
	7	2105 – 2155	0.81	110
Ocean Color	8	405 – 420	0.33	880
	9	438 – 448	0.23	838
	10	483 – 493	0.17	802
	11	526 – 536	0.15	754
	12	546 – 556	0.12	750
	13	662 – 672	0.08	910
	14	673 – 683	0.07	1087
	15	743 – 753	0.07	586
	16	862 – 877	0.06	516

atmosphere [10]. One set of MODIS channels, i.e., Channels 8–16, in the 0.4–0.9 μm spectral range is designed mainly for remote sensing of Case 1 waters. Another set of channels, i.e., Channels 1–7, in the 0.4–2.3 μm region is designed for the remote sensing of land and atmosphere but also has applications for remote sensing of coastal and inland waters. Table I lists the main characteristics of the relevant MODIS channels [4]. The ocean color channels have much higher signal-to-noise ratios and are sensitive to darker surfaces than the land channels centered at similar wavelengths. However, the ocean color channels can saturate over bright targets because the maximum reflectances specified for these channels are significantly smaller than those for the land channels at similar wavelengths. Fig. 1(a) shows a true color image processed from three MODIS land channels (red: Channel 1; green: Channel 4; blue: Channel 3). The image was degraded to the 1-km spatial resolution of ocean color channels. The original spatial resolutions for land Channels 1, 4, and 3 are 250, 500, and 500 m, respectively. The Aqua MODIS imagery was measured on March 6, 2004 over the Bahamas Banks centered near 24.8° N and 78.1° W. The elongated Andros Island is seen as the bright white area in the middle left portion of the image. The shallow sediment banks to the west of Andros Island are seen as series of streaks. Fig. 1(b) shows the true color image processed from three MODIS ocean color channels (red: Channel 13; green: Channel 12; blue: Channel 10) at a spatial resolution of 1 km for the same scene. Many of the spatial features observed with imagery produced from the land channels such as the shallow sediment banks cannot be observed with the ocean channels, which saturate over bright water surfaces. This demonstrates that the MODIS ocean color channels are not adequate for the remote sensing of bright coastal waters, while the MODIS land channels can be useful for such purposes.

III. RADIATIVE TRANSFER MODELING AND RETRIEVALS

A. *Hyperspectral Atmospheric Correction Algorithm*

Because water-leaving radiances in the 0.66–0.76 μm spectral region over optically shallow or turbid coastal waters can be significantly greater than zero due to scattering by the bottom or suspended materials [11], we derive aerosol information from a spectrum-matching algorithm that uses channels in longer wavelengths (where water-leaving radiances are closer to zero) in our previously developed hyperspectral atmospheric correction algorithm [9]. The aerosol information is extrapolated back to the visible spectral range based on the selected aerosol models for the retrieval of water-leaving radiances. The algorithm has been tested with hyperspectral imagery acquired with the Airborne Visible Infrared Imaging Spectrometer (AVIRIS) [12] from an ER-2 aircraft at an altitude of 20 km over Monterey Bay [13]. AVIRIS has two hundred twenty-four 10-nm channels covering the entire 0.4–2.5 μm wavelength region with a high spatial resolution of 20 m. The algorithm has also been successfully used to atmospherically correct high-resolution airborne imagery from the Portable Hyperspectral Imager for Low-Light Spectroscopy [14] collected from an altitude of 3 km over the Bahamas [15], [16].

In the hyperspectral algorithm, we work with reflectances. We adopt the standard definition of apparent reflectance $\rho^*_{\rm obs}$ at a satellite level for a given wavelength as

$$\rho^*_{\rm obs} = \pi L_{\rm obs}/(\mu_o F_o) \tag{1}$$

where $L_{\rm obs}$ is the radiance of the ocean–atmosphere system measured by a satellite instrument, μ_o is the cosine of the solar zenith angle, and F_o is the extraterrestrial downward solar irradiance at the top of the atmosphere when the solar zenith angle is equal to zero [17]. Neglecting the interactions between atmospheric gaseous absorption and molecular and aerosol scattering, $\rho^*_{\rm obs}$ can be expressed as [9], [18]

$$\rho^*_{\rm obs} = T_g \left[\rho^*_{\rm atm+sfc} + \rho_w t_d t_u/(1 - s\rho_w)\right] \tag{2}$$

where T_g is the total atmospheric gaseous transmittance on the sun-surface–sensor path, $\rho^*_{\rm atm+sfc}$ is the reflectance resulting from scattering by the atmosphere and specular reflection by ocean surface facets, t_d is the downward transmittance (direct + diffuse), t_u is the upward transmittance, s is the spherical albedo that takes into account the reflectance of the atmosphere for isotropic radiance incident at its base, and ρ_w is the water-leaving reflectance. Solving (2) for ρ_w yields

$$\rho_w = \left(\rho^*_{\rm obs}/T_g - \rho^*_{\rm atm+sfc}\right)/\left[t_d t_u + s\left(\rho^*_{\rm obs}/T_g - \rho^*_{\rm atm+sfc}\right)\right]. \tag{3}$$

Given $L_{\rm obs}$, the water-leaving reflectance can be derived according to (1) and (3) provided that the other quantities in the right hand side of (3) can be modeled theoretically.

We use a modified version of the Ahmad and Fraser code [19] to generate lookup tables for retrieving the required

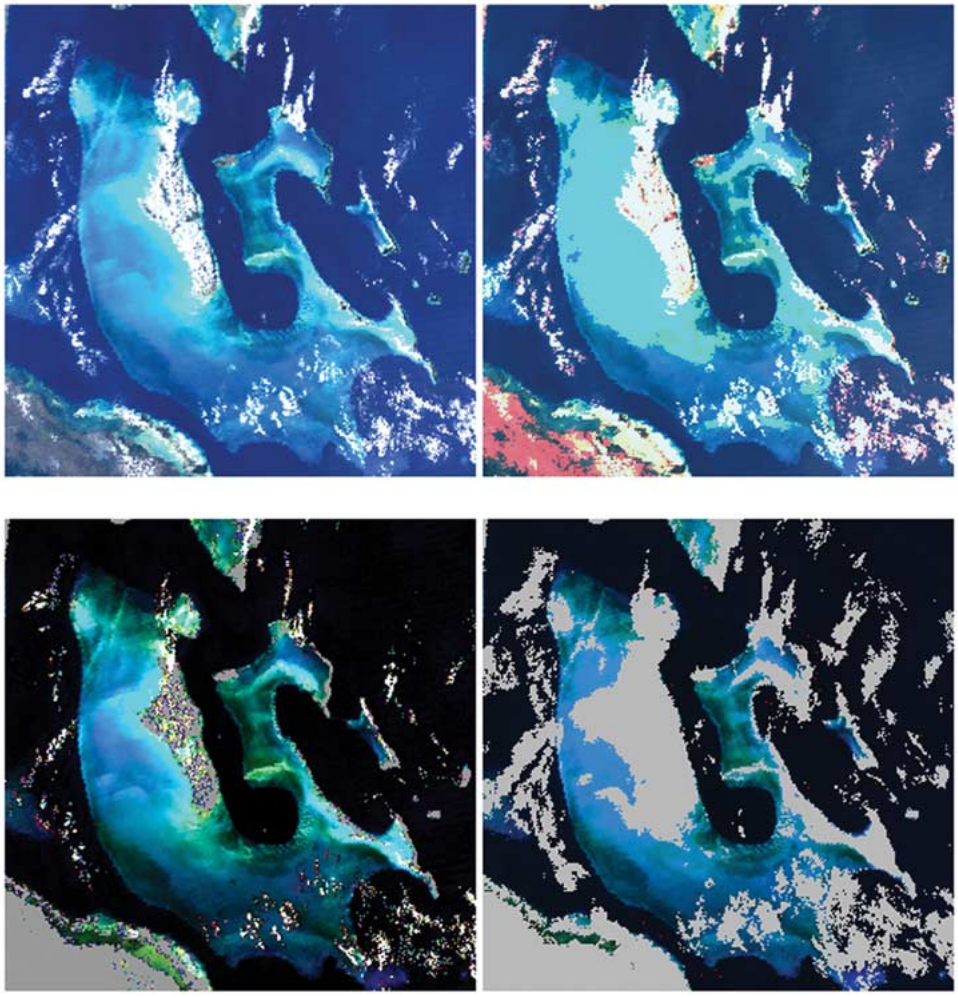

Fig. 1. (a) Color image of three MODIS land channels (red: Channel 1; green: Channel 4; blue: Channel 3) acquired on March 6, 2004 over the Bahamas. (b) Color image of three MODIS ocean color channels (red: Channel 13, green: Channel 12; blue: Channel 10). (c) Water-leaving reflectance image of the three land channels derived with our atmospheric correction algorithm. (d) Water-leaving reflectance image of the three ocean color channels derived with the MODIS operational atmospheric correction algorithm. Andros Island is the large island just left of the center of the image. Gray areas in (c) and (d) are areas that did not give usable ocean radiances because of land, clouds, or negative radiances.

atmospheric parameters. This code includes an atmospheric layering structure that allows for the proper mixing of aerosol particles with atmospheric molecules and the treatment of wind-roughened water surfaces. Specifically, the lookup tables are used to derive the quantities $\rho^*_{\mathrm{atm+sfc}}$, t_d, t_u, and s, and have been generated for 14 wavelengths coinciding with atmospheric "window" regions (0.39, 0.41, 0.44, 0.47, 0.51, 0.55, 0.61, 0.67, 0.75, 0.865, 1.04, 1.24, 1.64, and 2.25 μm), sets of aerosol models, optical depths, solar and view angles, and surface wind speeds [9]. Aerosol models, which are similar to those used by Gordon and Wang [7] plus five absorbing aerosol models [20], are used during our table generation. A line-by-line-based atmospheric transmittance code is used to calculate contiguous atmospheric gaseous transmittance spectra (T_g) [21].

B. Multichannel Atmospheric Correction Algorithm

During the NASA-sponsored Sensor Intercomparison and Merger for Biological and Interdisciplinary Ocean Studies program [22], we modified the hyperspectral atmospheric correction algorithm for processing multichannel imagery such as those acquired with the Terra and Aqua MODIS instruments and produced a multichannel version of atmospheric correction code. During the updating processes, lookup tables corresponding to the 16 MODIS channels listed in Table I are obtained through linear interpolation of the tables generated for the hyperspectral atmospheric correction algorithm. The lookup table quantities $\rho^*_{\mathrm{atm+sfc}}$, t_d, t_u, and s are functions of wavelength (λ), solar zenith angle (θ_o), view zenith angle (θ), relative azimuth angle $(\phi - \phi_o)$, aerosol model, optical depth (τ_a), and surface wind speed (W). The values of $\rho^*_{\mathrm{atm+sfc}}$ in our multichannel lookup table are obtained for a total of 25 aerosol models, 16 MODIS channels, and for the following values of independent variables:

τ_a 0, 0.1, 0.2, 0.3, 0.5, 0.7, 1.0, 1.3, 1.6, and 2.0 at 0.55 μm;
θ_o 1.5°, 12°, 24°, 36°, 48°, 54°, 60°, 66°, and 72°;
θ 0°, 1.5°, 6°, 12°, 18°, 24°, 30°, 36°, 42°, 48°, 54°, 60°, 66°, 72°, 78°, 84°, and 88.5°;
ϕ_o 0;
ϕ 0°, 12°, 24°, 36°, 48°, 60°, 72°, 84°, 90°, 96°, 108°, 120°, 132°, 144°, 156°, 168°, and 180°;
W 2, 6, and 10 m/s;

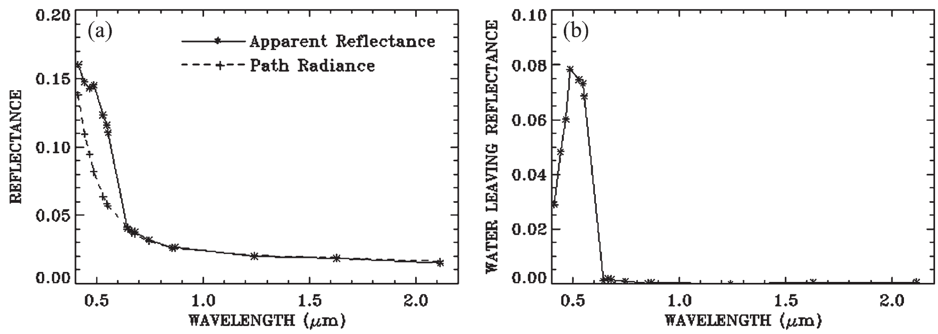

Fig. 2. (a) Illustration of the spectrum-matching technique for estimating reflectances due to atmospheric scattering and specular surface reflection for an Aqua MODIS water pixel. (b) Estimated water-leaving reflectances for the pixel. See text for detailed descriptions.

where the τ_a values are aerosol optical depths at 0.55 μm. The selection of step sizes for these parameters was based on the work of Fraser *et al.* [23].

For MODIS data, each pixel's solar zenith angle, view zenith angle, and relative azimuth angle is variable because of the large swath width ($\sim$2800 km for one scan line). The MODIS lookup tables need to be interpolated to the solar and view geometry appropriate for each pixel. This can be far more time consuming than for processing the high spatial resolution ($\sim$30 m) hyperspectral imaging data in which the solar and viewing angles can be assumed to be constant for thousands of pixels. To speed up the interpolation process, the storage order for the MODIS lookup table quantities is optimized. After the optimization, the storage order for $\rho^*_{\mathrm{atm+sfc}}$ becomes wavelength, optical depth, aerosol model, solar zenith angle, relative azimuth angle, and view zenith angle. The required time for processing one MODIS data set decreases from several hours to several minutes on an SGI workstation.

The spectrum-matching routines [9] have been improved. A minimization procedure, which is similar to a golden search [24], has been implemented to refine the estimates of aerosol optical depths. Because the parameters stored in the lookup tables have coarse intervals (see descriptions above), the lookup tables are interpolated automatically during the minimization process. The absorbing aerosols have effects at wavelengths shorter than about 0.7 μm. To avoid possible confusion in aerosol model selections using channels at 0.86 μm or longer wavelengths, the 20 nonabsorbing aerosol models are normally used for spectrum matching, while the five absorbing aerosol models are not. If the absorbing aerosols are known to be present, for example, based on ground-based upward-looking sun photometer measurements, one can select the five absorbing aerosol models during the spectrum-matching process.

Several masks such as the land/water mask, cloud mask, glint mask, and thin cirrus mask have also been implemented into the algorithm to identify water pixels for processing. The simple land/water mask is based on the normalized difference vegetation index (NDVI) [25], [26]. Most water pixels have negative NDVI values, while land pixels have positive NDVI values. This may not be the case for dense accumulations of phytoplankton at the sea surface (i.e., red tides). The cloud mask is based on the 1.24-μm channel apparent reflectances. The thin cirrus mask is based on the apparent reflectances of the 1.38-μm channel [27], [28]. The threshold values for these masks can be adjusted by the users of the algorithm.

Fig. 2 shows an example of spectrum matching for the derivation of water-leaving reflectances from MODIS data. The points marked with the symbol "*" in Fig. 2(a) are the measured apparent reflectances from Aqua MODIS for a water pixel. The solid line that connects these points only serves as a guide to the eye. There are no real measured data between those marked points because MODIS is a multichannel radiometer without contiguous spectral coverage. The points marked with the "+" symbol are our estimated reflectances due to atmospheric scattering and specular surface reflection. During the estimating process, the water-leaving reflectances for the three MODIS land channels centered near 0.865 μm (Channel 2), 1.24 μm (Channel 5), and 2.13 μm (Channel 7) are assumed to be zero. An aerosol model and an optical depth are derived by minimizing the differences between measured and predicted reflectances for the three channels. The aerosol transmittances and path radiances are extracted back to the visible spectral range based on the estimated aerosol properties from the near-IR channels. The water-leaving reflectances in the visible spectral range for the pixel are derived according to (3) and shown in Fig. 2(b). Because nearly half of the detectors for the Aqua MODIS channel centered near 1.64 μm (Channel 6) are not functioning, this channel is infrequently used during retrievals.

IV. Sample Results

The multichannel version of the atmospheric correction algorithm has been applied to Terra and Aqua MODIS data sets measured over optically shallow and turbid coastal waters in different geographical regions. Here, we present the results from applications of the algorithm to two different Case 2 water regions. Field measurements of water-leaving reflectances are available for the Aqua MODIS imagery acquired on March 6, 2004 and July 7, 2005 over the southern Florida and Bahamas areas. A description of the selected field stations can be found in Table II, and the station locations are illustrated in Fig. 3. Stations were selected to demonstrate retrievals for a wide variety of bottom types. Only stations with relatively uniform bottoms were used so that the point samples could be compared with the retrievals from the approximately 1-km^2 MODIS pixels.

TABLE II
DESCRIPTIONS OF SELECTED FIELD STATIONS IN BAHAMAS BANKS AND FLORIDA BAY

Station	Latitude	Longitude	Date	Bottom Depth (m)	Seafloor Description
Bahamas Banks					
1	25°48.236’N	79°06.776’W	3/14/2004	5.0	Moderate seagrass
5	25°48.680’N	76°46.304’W	3/19/2004	5.6	Algal grapestone sediment
8	24°13.875’N	76°31.233’W	3/20/2004	5.0	Sparse seagrass
18	25°07.033’N	78°28.423’W	3/28/2004	5.0	White sediment
Florida Bay					
2	24°52.610’N	80°57.53’W	6/27/2005	0.85	Dense serengodium
3	24°51.000’N	81°0.522’W	6/28/2005	1.61	Dense seagrass
8	24°54.000’N	80°58.997’W	7/1/2005	2.25	Dense seagrass
13	25°01.952’N	81°3.508’W	7/5/2005	2.89	Sandy sediment

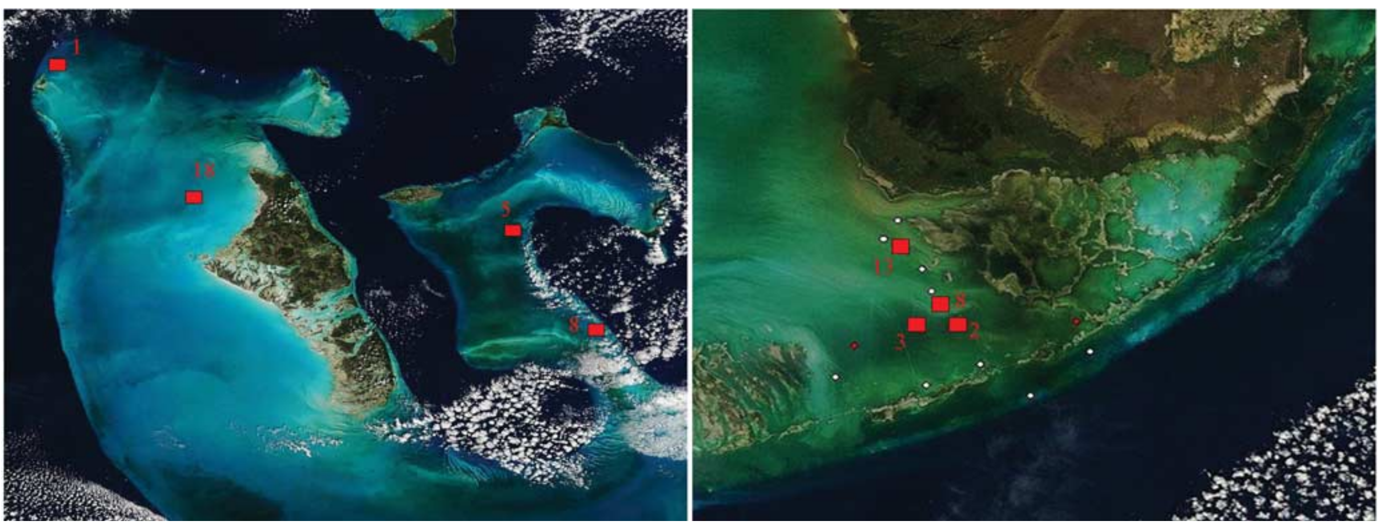

Fig. 3. Locations of the selected field stations in (a) Bahamas Banks and (b) Florida Bay. The MODIS pseudo true color image from January 21, 2003, which was derived from a combination of the 250- and 500-m land channels, was selected because of the minimal cloud contamination over both regions.

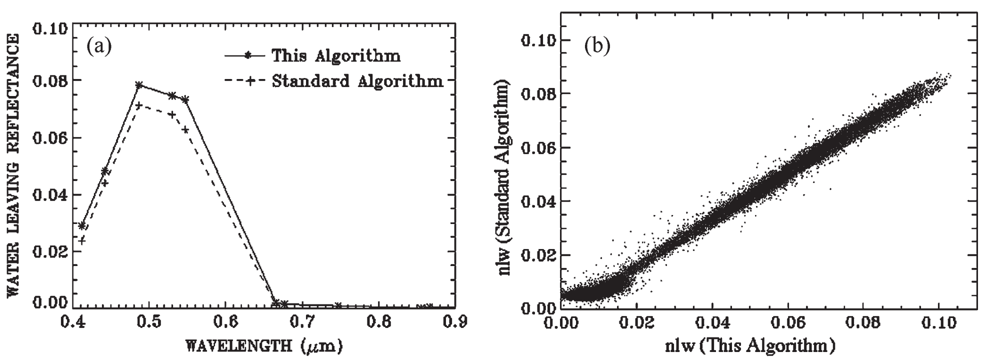

Fig. 4. (a) Comparison between water-leaving reflectances over an optically deep water pixel derived with the standard MODIS algorithm and this algorithm. (b) Scatter plot of Channel 12 (0.546–0.556 mm) water-leaving reflectances derived with the two algorithms for all the pixels in Fig. 1(d) over which both algorithms had retrievals.

Bahamas Banks is generally characterized by clear Case 1 waters but is optically complex, or Case 2, because light reflected from the seafloor contributes significantly to the water-leaving reflectance. The seafloor composition varies from bright sand to dense sea grass [15]. The land channel and ocean color channel images for the March 6, 2004 Bahamas Banks data set are already shown in Fig. 1(a) and (b), respectively. Fig. 1(c) shows our atmosphere-corrected image for the three land

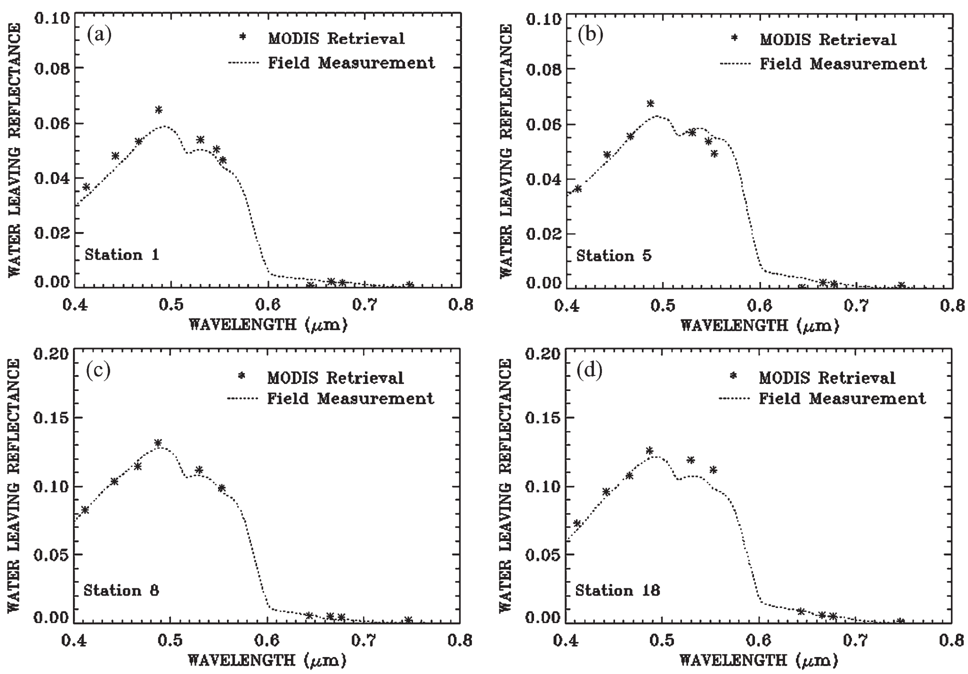

Fig. 5. Comparisons between water-leaving reflectances retrieved with our algorithm and those measured with a portable field spectrometer over four surface stations in Bahamas Banks.

channels. Water-leaving reflectances over most bright water pixels are retrieved. The spatial patterns of water-leaving reflectances over bright water areas are contiguous. Fig. 1(d) shows the water-leaving reflectances for the three ocean color channels derived with the MODIS operational ocean color algorithm. Most of the bright water pixels are masked out either because of the saturation of ocean color channels or the inability of the operational algorithm for deriving water-leaving reflectances over the pixels.

By comparing Fig. 1(c) with Fig. 1(d), it is seen that both our multichannel algorithm and the standard MODIS operational algorithm have retrievals over deeper ocean waters, where the bottom reflectances do not cause saturations of MODIS ocean color channels. Fig. 4(a) shows an example of retrievals from both algorithms over a pixel. The absolute values of water-leaving reflectances in the visible spectral region derived with the two algorithms differ slightly. The shapes of the two curves in Fig. 4(a) are quite similar. Many factors can cause differences in retrieval results. For example, the lookup tables used in the two algorithms are generated with two separate atmospheric radiative transfer programs. The two algorithms use different atmospheric correction channels. The standard MODIS operational algorithm allows the fine tuning of radiometric calibration coefficients, while our algorithm does not. The agreement between the two retrievals in Fig. 4(a) is actually quite good in view of these factors that can potentially cause significant differences in retrieval results. To compare the two retrievals over an extended area, we show in Fig. 4(b) a scatter plot of water-leaving reflectances retrieved with both algorithms for Channel 12 (bandwidth: 0.546–0.556 μm) and for all the Fig. 1(d) pixels over which both algorithms had retrievals. The results from the two retrievals are linearly related. A line with a slope of 0.92 fits the points with water-leaving reflectances greater than about 0.02.

Fig. 5 shows comparisons between water-leaving reflectances retrieved with our algorithm and those measured with a field spectrometer (Field Spec Pro VNIR-NIR1 portable spectrometer system from Analytical Spectral Devices) over four water targets in the Bahamas Bank areas. Our retrieved reflectances agree quite well in magnitude and spectral shape with those from field measurements. The field measurements and subsequent data reduction were made using well-established procedures [29], [30]. Because the field of view of the portable spectrometer is on the order of 1 m while the size of the MODIS pixel is 1 km or larger, the agreement between the two types of measurements should be considered to be qualitative in nature. Since our algorithm can recover water-leaving reflectances over bright water pixels whereas the MODIS operational algorithm cannot, our algorithm is complementary to the operational algorithm for coastal water applications.

In contrast to Bahamas Banks, Florida Bay has more turbid waters comprised of mixtures of phytoplankton, colored dissolved organic matter, and suspended sediment. Fig. 6 illustrates the water-leaving radiance retrievals from the Aqua MODIS data measured over Florida Bay on July 7, 2005. Water features (blue and light green) in the Florida Key areas are seen in the lower portion of Fig. 6(a) in the land channel image. Major portions of these features become white in the ocean color channel image in Fig. 6(b) because of the saturation problems associated with MODIS ocean color channels. With the application of our algorithm, water-leaving reflectances of MODIS land channels over the Florida Key areas, except cloudy pixels, are retrieved and shown in Fig. 6(c). Ocean

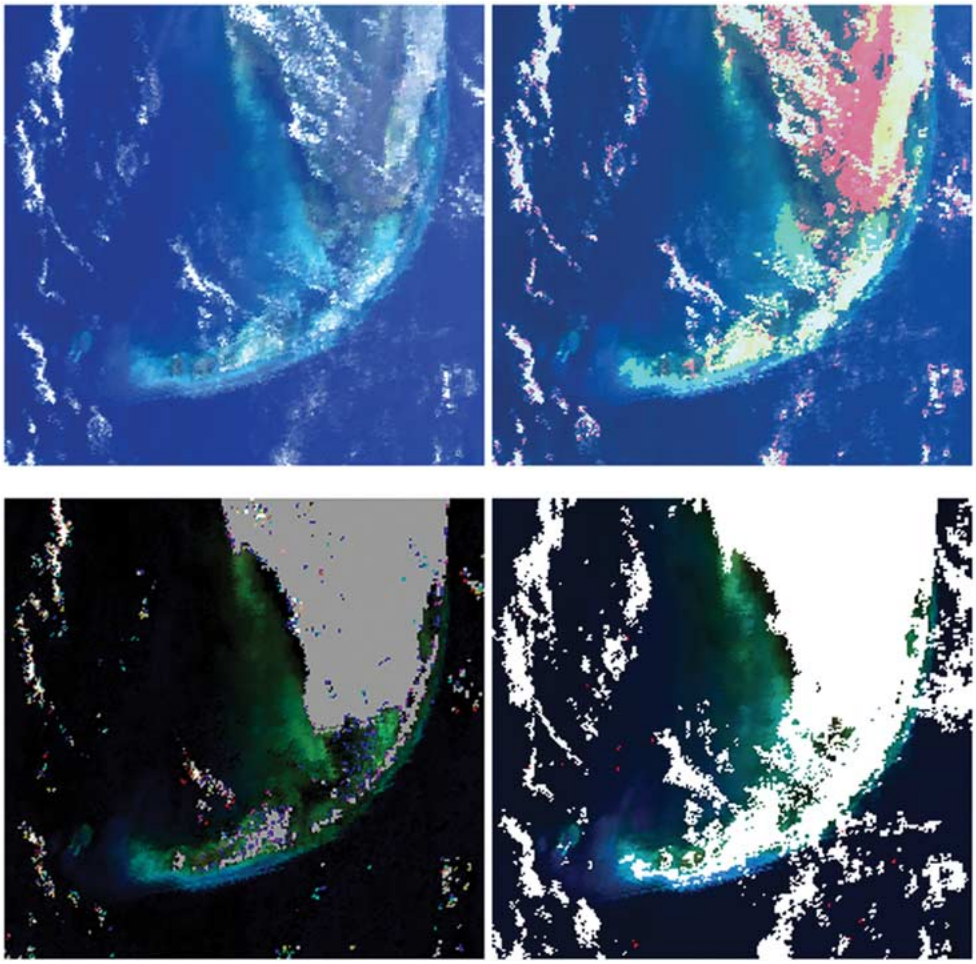

Fig. 6. (a) Color image of three MODIS land channels (red: Channel 1; green: Channel 4; blue: Channel 3) acquired on July 7, 2005 over the Florida Bay areas. (b) Color image of three MODIS ocean color channels (red: Channel 13, green: Channel 12; blue: Channel 10). (c) Water-leaving reflectance image of the three land channels derived with our atmospheric correction algorithm. (d) Water-leaving reflectance image of the three ocean color channels derived with the MODIS operational atmospheric correction algorithm.

color patterns over major portions of the Florida Key areas disappear in the water-leaving reflectance image of the ocean color channels retrieved with the MODIS operational algorithm [Fig. 6(d)]. These figures demonstrate again the ability of our algorithm in recovering water-leaving reflectances over bright waters where the MODIS operational algorithm cannot. Fig. 7 shows comparisons between our retrievals of water-leaving reflectances and field measurements over four water targets in the Florida Key areas. Again, the retrieval results and field measurements agree well. The agreement should also be considered to be qualitative in nature because MODIS and the portable spectrometer have very different pixel sizes, and the field measurements were not made simultaneously with the MODIS data acquisition.

V. Discussion

The aerosol models used in our generation of lookup tables are derived from the 1979 Shettle and Fenn [31] tropospheric and oceanic aerosols. The same types of aerosol models were previously used to generate lookup tables for the operational SeaWiFS atmospheric correction algorithm [7]. Extensive comparisons [32] of the aerosol optical properties, i.e., the optical depth at 0.55 μm and the spectral dependence of aerosols, derived from a time series of SeaWiFS data set with those from other aerosol measurements have demonstrated that the Shettle and Fenn aerosol models are quite suited for aerosol retrievals over the ocean. On the other hand, Smirnov *et al.* [33] have recently reported that the Shettle and Fenn tropospheric aerosol model is too broad based on the analysis of ground-based upward-looking sun photometer measurements over five geographic locations in the ocean. Because systematic errors in the assumed aerosol models will introduce errors in the derived water-leaving reflectance from remotely sensed data, further research on atmospheric aerosol models and their suitability for use in atmospheric correction algorithms should be made in the future.

VI. Summary

We have developed an atmospheric correction algorithm for multichannel remote sensing of ocean color. The algorithm uses channels located at wavelengths longer than 0.8 μm for estimates of aerosol models and optical depths. The aerosol

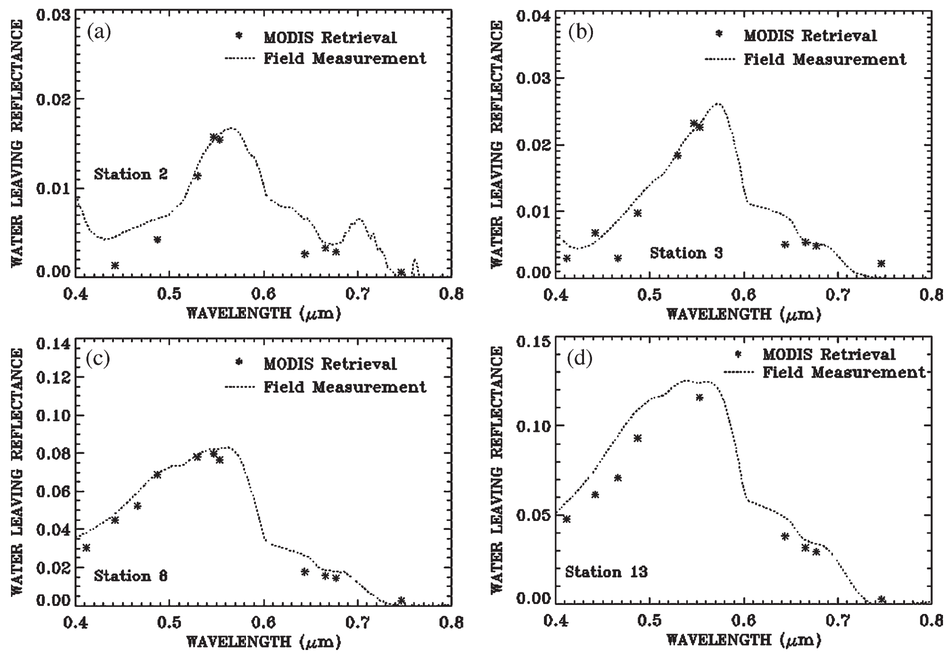

Fig. 7. Comparisons between water-leaving reflectances retrieved with our algorithm and those measured with a portable field spectrometer over four surface stations in Florida Bay areas.

information is extracted back to the shorter wavelength visible channels (0.4–0.7 μm) during the retrieval of water-leaving reflectances. The algorithm was tested with imagery derived from the MODIS ocean color sensor. Through limited case studies, we have found that the water-leaving reflectance retrievals with our algorithm over deep ocean waters agree with those derived with the MODIS operational atmospheric correction algorithm. Our retrieved water-leaving reflectances over brighter coastal waters agree with a selection of field measurements made in both Bahamas Banks and Florida Bay. Because the MODIS operational algorithm cannot be used for the retrieval of water-leaving reflectances over brighter coastal waters, our algorithm can be used as an alternative atmospheric correction algorithm for coastal water applications.

Acknowledgment

The authors would like to thank R. Zimmerman and his laboratory for the collection of field data, the crew onboard *R/V Walton Smith*, and the staff at Keys Marine Laboratory, Florida.

References

[1] H. R. Gordon, "Removal of atmospheric effects from satellite imagery of the oceans," *Appl. Opt.*, vol. 17, no. 10, pp. 1631–1636, May 1978.

[2] S. B. Hooker, W. E. Esaias, G. C. Feldman, W. W. Gregg, and C. R. McClain, "An overview of SeaWiFS and ocean color," NASA Goddard Space Flight Center, Greenbelt, MD, SewWiFS Tech. Rep. NASA Tech. Memo. 104566, 1992, vol. 1.

[3] V. V. Salomonson, W. L. Barnes, P. W. Maymon, H. E. Montgomery, and H. Ostrow, "MODIS: Advanced facility instrument for studies of the Earth as a system," *IEEE Trans. Geosci. Remote Sens.*, vol. 27, no. 2, pp. 145–153, Mar. 1989.

[4] M. D. King, Y. J. Kaufman, W. P. Menzel, and D. Tanre, "Remote sensing of cloud, aerosol, and water vapor properties from the Moderate Resolution Imaging Spectrometer (MODIS)," *IEEE Trans. Geosci. Remote Sens.*, vol. 30, no. 1, pp. 2–27, Jan. 1992.

[5] H. Kawamura and the OCTS Team, "OCTS mission overview," *J. Oceanogr.*, vol. 54, no. 5, pp. 383–399, 1998.

[6] A. Morel and L. Prieur, "Analysis of variations in ocean color," *Limnol. Oceanogr.*, vol. 22, no. 4, pp. 709–721, 1977.

[7] H. R. Gordon and M. Wang, "Retrieval of water leaving radiance and aerosol optical thickness over the oceans with SeaWiFS: A preliminary algorithm," *Appl. Opt.*, vol. 33, no. 3, pp. 443–452, Jan. 1994.

[8] C. D. Mobley, D. Stramski, W. P. Bissett, and E. Boss, "Optical modeling of ocean water: Is the Case 1—Case 2 classification still useful?" *Oceanography*, vol. 17, no. 2, pp. 60–67, 2004.

[9] B.-C. Gao, M. J. Montes, Z. Ahmad, and C. O. Davis, "Atmospheric correction algorithm for hyperspectral remote sensing of ocean color from space," *Appl. Opt.*, vol. 39, no. 6, pp. 887–896, Feb. 2000.

[10] M. D. King, W. P. Menzel, Y. J. Kaufman, D. Tanre, B.-C. Gao, S. Platnick, S. A. Ackerman, L. A. Remer, R. Pincus, and P. A. Hubanks, "Cloud and aerosol properties, precipitable water, and profiles of temperature and humidity from MODIS," *IEEE Trans. Geosci. Remote Sens.*, vol. 41, no. 2, pp. 442–458, Feb. 2003.

[11] R.-R. Li, Y. J. Kaufman, B.-C. Gao, and C. O. Davis, "Remote sensing of suspended sediments and shallow coastal waters," *IEEE Trans. Geosci. Remote Sens.*, vol. 41, no. 3, pp. 559–566, Mar. 2003.

[12] G. Vane, R. O. Green, T. G. Chrien, H. T. Enmark, E. G. Hansen, and W. M. Porter, "The airborne visible/infrared imaging spectrometer," *Remote Sens. Environ.*, vol. 44, no. 2/3, pp. 127–143, 1993.

[13] J. Ryan, H. M. Dierssen, R. M. Kudela, C. A. Scholin, K. S. Johnson, J. Sullivan, A. M. Fischer, E. Rienecker, P. McEnaney, and F. P. Chavez, "Coastal ocean physics and red tides: An example from Monterey Bay, California," *Oceanography*, vol. 18, no. 2, pp. 246–255, 2005.

[14] C. O. Davis *et al.*, "Ocean PHILLS hyperspectral imager: Design, characterization, and calibration," *Opt. Express*, vol. 10, no. 4, pp. 210–221, Feb. 2002.

[15] H. M. Dierssen, R. C. Zimmerman, R. A. Leathers, T. V. Downes, and C. O. Davis, "Ocean color remote sensing of seagrass and bathymetry in the Bahamas Banks by high resolution airborne imagery," *Limnol. Oceanogr.*, vol. 48, no. 1, pp. 444–455, 2003.

[16] E. M. Louchard, R. P. Reid, C. F. Stephens, C. O. Davis, R. A. Leathers, and T. V. Downes, "Optical remote sensing of benthic habitats and bathymetry in coastal environments at Lee Stocking Island, Bahamas: A comparative spectral classification approach," *Limnol. Oceanogr.*, vol. 48, no. 1, pp. 511–521, 2003.

[17] H. R. Gordon and K. J. Voss, *MODIS Normalized Water-Leaving Radiance Algorithm Theoretical Basis Document (MOD 18)*, 1999. NASA Report NAS5-31363.

[18] D. Tanre, C. Deroo, P. Duhaut, M. Herman, and J. J. Morcrette, "Description of a computer code to simulate the satellite signal in the solar

spectrum: The 5S code," *Int. J. Remote Sens.*, vol. 11, no. 4, pp. 659–668, 1990.
[19] Z. Ahmad and R. S. Fraser, "An iterative radiative transfer code for ocean–atmosphere systems," *J. Atmos. Sci.*, vol. 39, no. 3, pp. 656–665, Mar. 1982.
[20] M. J. Montes, B.-C. Gao, and C. O. Davis, "New algorithm for atmospheric correction of hyperspectral remote sensing data," *Proc. SPIE*, vol. 4383, pp. 23–30, Jun. 2001.
[21] B.-C. Gao and C. O. Davis, "Development of a line-by-line-based atmosphere removal algorithm for airborne and spaceborne imaging spectrometers," *Proc. SPIE*, vol. 3118, pp. 132–141, Oct. 1997.
[22] C. McClain, W. Esaias, G. Feldman, R. Frouin, W. Gregg, and S. Hooker, *The Proposal for the NASA Sensor Intercalibration and Merger for Biological and Interdisciplinary Oceanic Studies (SIMBIOS) Program, 1995*, 2002, Greenbelt, MD: NASA Goddard Space Flight Center. NASA Tech. Memo. 2002-210008, 54pp.
[23] R. S. Fraser, S. Mattoo, E.-N. Yeh, and C. R. McClain, "Algorithm for atmospheric and glint corrections of satellite measurements of ocean pigment," *J. Geophys. Res.*, vol. 102, no. D14, pp. 17 107–17 118, 1997.
[24] W. H. Press, S. A. Teukolsky, W. T. Vetterling, and B. R. Flannery, *Numerical Recipes in FORTRAN The Art of Scientific Computing*, 2nd ed. Cambridge, U.K.: Cambridge Univ. Press, 1992, p. 963.
[25] D. W. Deering, "Rangeland reflectance characteristics measured by aircraft and spacecraft sensors," Ph.D. dissertation, Texas A & M Univ., College Station, TX, 1978. 338 pp.
[26] C. J. Tucker, C. O. Justice, and S. D. Pince, "Monitoring the grasslands of the Sahel 1984–1985," *Int. J. Remote Sens.*, vol. 7, no. 11, pp. 1571–1581, 1986.
[27] B.-C. Gao and Y. J. Kaufman, "Selection of the 1.375-μm MODIS channel for remote sensing of cirrus clouds and stratospheric aerosols from space," *J. Atmos. Sci.*, vol. 52, no. 23, pp. 4231–4237, Dec. 1995.
[28] B.-C. Gao, P. Yang, W. Han, R.-R. Li, and W. J. Wiscombe, "An algorithm using visible and 1.38-micron channels to retrieve cirrus cloud reflectances from aircraft and satellite data," *IEEE Trans. Geosci. Remote Sens.*, vol. 40, no. 8, pp. 1659–1668, Aug. 2002.
[29] J. T. O. Kirk, *Light and Photosynthesis in Aquatic Ecosystems*. Cambridge, U.K.: Cambridge Univ. Press, 1994.
[30] C. D. Mobley, "Estimation of the remote sensing reflectance from above-surface measurements," *Appl. Opt.*, vol. 38, no. 36, pp. 7442–7455, Dec. 1999.
[31] E. P. Shettle and R. W. Fenn, *Models for the Aerosols of the Lower Atmosphere and the Effects of Humidity Variations on Their Optical Properties*. Hanscom, MA: U.S. Air Force Geophys. Lab., Hanscom Air Force Base, 1979.
[32] M. H. Wang, K. D. Knobelspiesse, and C. R. McClain, "Study of the sea-viewing wide field-of-view sensor (SeaWiFS) aerosol optical property data over ocean in combination with the ocean color products," *J. Geophys. Res.*, vol. 110, no. D10, D10S06, 2005. DOI:10.1029/2004JD004950.
[33] A. Smirnov, B. N. Holben, Y. J. Kaufman *et al.*," Optical properties of atmospheric aerosol in maritime environments," *J. Atmos. Sci.*, vol. 59, no. 3, pp. 501–523, Feb. 2002.

Bo-Cai Gao received the B.S. degree from Nankai University, Tianjin, China, in 1982 and the M.S. and Ph.D. degrees from Ohio State University, Columbus, in 1984 and 1988, respectively, all in physics.

He is currently with the Remote Sensing Division, Naval Research Laboratory, Washington, DC. He is a member of the MODIS Science Team, where his focus is on the remote sensing of cirrus clouds, atmospheric water vapor, and coastal water.

Dr. Gao received the Prize Paper Award from the IEEE Geoscience and Remote Sensing Society in 1991 for his development of an operational atmospheric radiative transfer code to retrieve surface reflectance spectra from hyperspectral imaging data measured with the NASA/JPL Airborne Visible/Infrared Imaging Spectrometer.

Marcos J. Montes received the B.S. degree in physics and mathematics from New Mexico State University, Las Cruces, in 1987 and the Ph.D. degree in physics from Stanford University, Stanford, CA, in 1996.

He is currently with the Remote Sensing Division, Naval Research Laboratory, Washington, DC. He has conducted research in algorithms for the atmospheric correction of hyperspectral and multispectral remote sensing data acquired from aircraft and satellite platforms, and algorithms for retrieving internal optical properties of water and bottom reflectances.

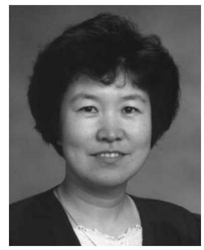

Rong-Rong Li received the B.S. degree in optical physics from Nankai University, Tianjin, China, in 1982 and the M.S. and Ph.D. degrees in physics from the University of Cincinnati, Cincinnati, OH, in 1989 and 1995, respectively.

She is currently with the Remote Sensing Division, Naval Research Laboratory, Washington, DC. She has conducted research in the remote sensing of atmospheric aerosols, water vapor, clouds, vegetation indices, fire, and coastal waters using multispectral and hyperspectral imaging data acquired from aircraft and satellite platforms.

Heidi Melita Dierssen completed her dissertation at the University of California, Santa Barbara, under the guidance of Dr. R. Smith, researching the bio-optical properties of Antarctic coastal waters. Her postdoctoral research involved the remote sensing of seagrass productivity in optically shallow water with R. Zimmerman at Moss Landing Marine Labs and evaluating the optics of red tides with J. Ryan at the Monterey Bay Aquarium Research Institute.

She is currently an Assistant Professor at the University of Connecticut, Groton. She is an Interdisciplinary Research Scientist who uses optics and remote sensing to address questions related to biological and physical processes in the ocean. She is a member of the NASA MODIS Science Team, the NASA Ocean Biology and Biogeochemistry Working Group, the NOAA Coastal Ocean Applications and Science Team, and has served as a planning member for several national science meetings. She has been involved in numerous large interdisciplinary projects involving multispectral and hyperspectral remote sensing, including the Palmer Long Term Ecological Research Project (Pal-LTER), Coastal Benthic Optical Properties (CoBOP) initiative, California State Universities Center for Integrative Coastal Observation, Research, and Education (CICORE), and the Long Island Sound Integrated Coastal Observing System (LISICOS). Her research has spanned the breadth of the world's oceans from the polar, temperate, and tropical seas, and her collaborators range from physical oceanographers to animal physiologists.

Curtiss O. Davis received the B.S. degree in zoology from the University of California, Berkeley, in 1966 and the Ph.D. degree in oceanography from the University of Washington, Seattle, in 1973.

He is currently a Senior Research Professor and the Associate Dean for research and facilities in the College of Oceanic and Atmospheric Sciences, Oregon State University, Corvallis. He was a Program Manager at the NASA Ocean Productivity Program from 1984 to 1986. He was a Research Oceanographer and Group Supervisor of the Biological and Polar Oceanography, Jet Propulsion Laboratory (JPL), Pasadena, CA, from December 1986 to March 1994. While at JPL, he was the Project Scientist for the High Resolution Imaging Spectrometer (HIRIS) from July 1990 to March 1994. In 1994, he was with the Naval Research Laboratory, Washington, DC, where he developed a program in the hyperspectral remote sensing of the coastal ocean. He was a member of the NASA SeaWiFS Science Team and has participated in numerous calibration and validation experiments. He was the Project Scientist for the Navy's Hyperspectral Remote Sensing Technology program, a focused effort to develop the use of hyperspectral imaging for the characterization of the coastal ocean.